Surface & Coatings Technology 205 (2011) 3087–3092

Contents lists available at ScienceDirect

Surface & Coatings Technology

journal homepage: www.elsevier.com/locate/surfcoat

Two-dimensional mapping of micro-hardness increase on surface treated steel determined by photothermal deflection microscopy

Ulises Crossa Archiopoli [a], Nélida Mingolo [a,*], Oscar E. Martínez [b,c]

[a] Universidad de Buenos Aires, Facultad de Ingeniería, Dto. Física, Buenos Aires, Argentina
[b] Universidad de Buenos Aires, Facultad de Ciencias Exactas, Dto. Física, Buenos Aires, Argentina
[c] CONICET, Argentina

ARTICLE INFO

Article history:
Received 22 June 2010
Accepted in revised form 8 November 2010
Available online 12 November 2010

Keywords:
Hardness
Surface characterization
Thermal diffusivity

ABSTRACT

An optical noncontact technique is presented that provides a two-dimensional map of the hardness of treated steel at the micrometer level. The photodeflection technique for determining the thermal diffusivity is shown to be a useful and rapid way to determine the hardness increase profile in two dimensions with only minor preparation of the sample (flat polish). This is possible due to the strong correlation found for this type of material between the inverse of the diffusivity and the hardness increment after treatment. The diffusivity retrieval is performed by a single measurement of the phase delay between the pump beam and the photodeflection signal thus allowing a rapid scanning of the surface. The surface scans of the hardness performed with this technique showed that anomalous regions can be identified that direct optical or scanning electron microscopy observation do not reveal.

1. Introduction

Distinct surface and bulk properties are required in most demanding applications of steel parts. Gradient properties are delivered to a thin layer of material and the characterization of such layer is mandatory but difficult and laborious. Particularly difficult is to determine the layer hardness profile in the micrometer level, requiring the use of nano-indenters [1], resulting in a time consuming, expensive technique that involves the participation of very skilled personnel. Even more expensive and time consuming is the determination of the phase structure by electron back-scattering diffraction [2]. Hence finding rapid and less expensive techniques that allow the correlation of the measured properties with the desired features such as structure and hardness is of permanent interest. Several works have been presented in the past decade relating the thermal diffusivity or conductivity with the hardness profile of a surface treated layer of steel samples in the millimeter range [3–12]. These works were based in the measurement of the temperature rise at the surface of the material, when periodically heated with a modulated light beam. As the frequency of modulation is reduced, a deeper layer is explored by the heat wave generated and sophisticated deconvolution methods were developed to retrieve the thermal diffusivity profile from the collected data. In this manner carburized and laser treated steel surfaces were characterized.

In this work we will present a different photothermal technique with microscopic resolution [13,14] that can retrieve the thermal diffusivity and the results will be correlated to the hardness profile measured with a nano-indenter. We will show that the technique is able to rapidly map the phase structure and hardness of surface treated steel samples. Moreover it will be shown that in our results and in prior other groups' work a unique straight line correlates the hardness increment due to the treatment with the increment in the inverse of the thermal diffusivity. The same correlation is obtained for carburized, laser quenched or electron beam melting and quenching.

2. Experimental

2.1. The sample

The sample was an AISI 4140 steel surface treated by single shot from a cold cathode electron gun [15–18] that transforms a layer a few microns thick to a metastable phase [19,20]. The base material was normalized according to the conventional cooling cycle for AISI 4140 steel alloy [21]. The gun consists of a pulsed glow discharge developed after establishing a high voltage at the cathode with a spark gap switch. Using a source voltage of 17 kV, the current pulsewidth was $\tau = 20\,\mu s$, the peak current 21 A and the beam area at the sample location was 10 mm^2.

A melt pool several microns thick is created after rapid heating of the surface due to electron bombardment, which rapidly cools dissipating heat against the substrate. A treated region several millimeters wide and tens of microns thick is produced.

* Corresponding author.
E-mail address: nmingol@fi.uba.ar (N. Mingolo).

0257-8972/$ – see front matter © 2010 Elsevier B.V. All rights reserved.
doi:10.1016/j.surfcoat.2010.11.022

The cooling rate computed from the numerical simulations is above 10^8 K/s at the beam centre. Different durations of the melted pool yield different textures that can be seen at the spot centre and at the first halo observed in the front view micrograph presented in Fig. 1.

A roughened surface appears due to Bènard–Marangoni instability [20] and has been shown to require a certain time to evolve [22]. The first halo also reaches the melting temperature but does not remain melted long enough for an instability to develop.

Grazing incidence X ray diffraction of both structures showed similar martensite content (50 vol.%) and a minor amount of retained austenite (between 5% and 10 vol.%) and F_3C (less than 2 vol.%) [22]. A transition layer appears in the cross section that corresponds to the second halo of the front view. This layer has been heated above the austenization temperature but does not melt. As a result it has lower martensite content (25 vol.%) than the surface layer and probably varies continuously towards the unaffected substrate (base material). The substrate is a pearlite structure.

For nano-hardness measurements a TriboIndenter® nanomechanical testing system (Hysitron Inc, MN, USA) with a Berkovich diamond indenter was used. Indentations were conducted in load-control mode applying a load-time cycle consisted in three load–unload sequences (900 μN/s), where the first two unload segments last at 10% of peak load which was equal to 4.5 mN. The last unload curve was chosen to obtain the hardness value following the Oliver and Pharr method [1].

In the present study the sample was cross sectioned, grinded and polished for nano-hardness and photothermal measurements. Previously, samples were nickel electroplated to produce a protective coating for polishing. For optical observations, it was necessary to etch the sample to reveal phases; the protocol is described in reference [22].

2.2. Photothermal method

The experimental setup is described in detail in reference [13] and [14]. A pump laser emitting at $\lambda = 532$ nm with an average power of 5 mW at the sample is modulated at the desired frequency (between 30 kHz and 5 MHz) and is focused on the sample surface by means of a microscope objective. A probe laser emitting at $\lambda = 690$ nm is focused besides the pump about one spot size away and the reflection is detected with a photodiode after the beam is clipped by the knife edge. Schematics of the mechanisms involved are illustrated in Fig. 2. The surface expands due to the heat absorbed from the modulated pump laser and the deformation deflects the probe beam, thus modifying the power detected by the photodiode after being clipped by the knife. A camera allows precise focusing, observation of the sample and measurement of the beam size.

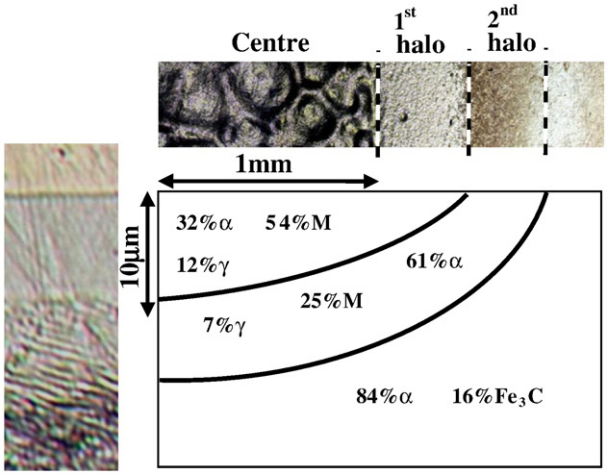

Fig. 1. Upper: front view, left: cross section of the treated sample. For optical metallographic observations the sample was etched [22]. The box shows schematically the characteristic dimensions of the HAZ (heated affected zone) and the phase content of the different layers as determined by grazing incidence X ray diffraction.

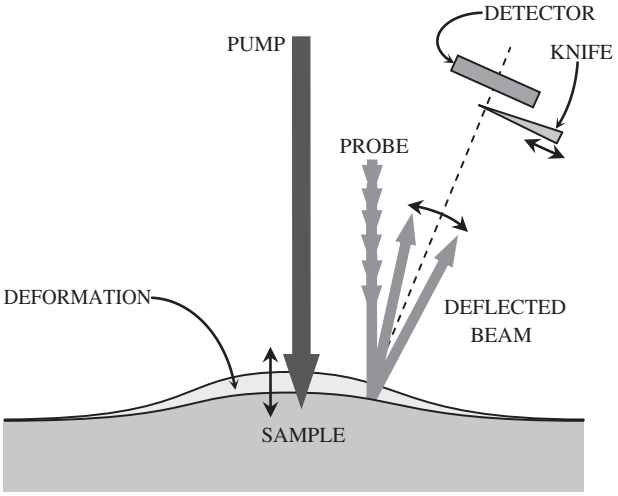

Fig. 2. Schematics of the mechanisms involved where it is shown that the surface expands due to the heat absorbed from the modulated pump laser and the deformation deflects the probe beam at the modulating frequency, thus modifying the power detected by the photodiode after being clipped by the knife.

In order to extract the modulated component both in amplitude and phase at the pump beam modulation frequency, a lock-in amplifier is used.

The signal is fitted considering the two mechanisms involved, change in reflectivity with temperature $A*f$ (thermoreflectance) and deflection $B*g$ (photodeflection) as described in detail in [13].

$$signal = A*f + B*g \tag{1}$$

Fig. 3 shows a typical behavior of the frequency dependence of the amplitude and phase of the signal. From the fit a critical frequency $\omega_0 = 2\pi f_0$ is retrieved that corresponds to that at which the heat

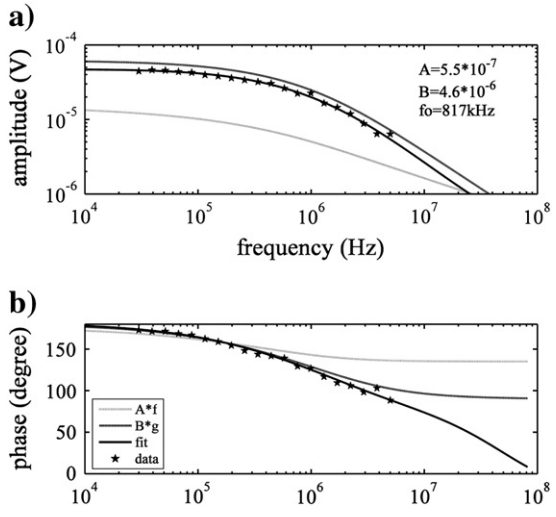

Fig. 3. Typical behavior of the frequency dependence of the amplitude and phase delay of the signal. $A*f$ and $B*g$ are the contributions to the signal from thermoreflectance and photodeflection respectively [13]. From the fit a critical frequency $\omega_0 = 2\pi f_0$ is retrieved that corresponds to that at which the heat diffuses a length equal to the pump beam size in one modulation period.

diffuses a length equal to the pump beam size in one modulation period, i.e.:

$$\omega_0 = \frac{2D}{\sigma^2} \tag{2}$$

where σ is the Gaussian pump beam size at the sample as defined in [14] and D is the thermal diffusivity of the sample.

The contribution from the probe beam deflection can be maximized by impinging at the sample with the probe displaced laterally respect to the pump at about one spot size away from the centre in the direction perpendicular to the knife edge. Under these conditions, as was shown in [14], the photodeflection signal has a much larger contribution than the thermoreflectance one, which can then be ignored (compare in Fig. 3a the data with the fit $B*g$). For this case the phase delay of the signal respect to the pump depends only on thermal diffusivity, beam sizes and relative position. If beam sizes and relative position are kept constant while the sample is scanned, a rapid retrieval of the critical frequency (and hence thermal diffusivity) can be obtained. This measurement condition makes the signal amplitude not relevant and hence is insensitive to reflectivity spatial variations. Defining the normalized beam displacement as:

$$xi = \frac{\Delta x}{\sigma} \tag{3}$$

where Δx is the displacement of the probe respect to the pump in the knife edge direction, and measuring at constant modulating frequency and constant xi, the thermal diffusivity can be retrieved from the phase delay, as discussed in [14]. In Fig. 4 the plot of normalized thermal diffusivity as a function of phase delay is presented for different values of xi. The parameter D' is defined as

$$D' = \frac{\omega\sigma^2}{2} \tag{4}$$

and is the thermal diffusivity for which the measuring frequency becomes critical as defined in Eq. (1). The plot shows that the maximum sensitivity is obtained when working at a frequency close to critical ($D/D' = 1$), where a 5% change in diffusivity yields a one degree change in phase delay. Calibration of thermal diffusivity as a function of phase delay is performed by making a complete fit of a frequency scan similar to that shown in Fig. 3 at a few points of the sample as described in [14] and is shown in the Fig. 4 inset.

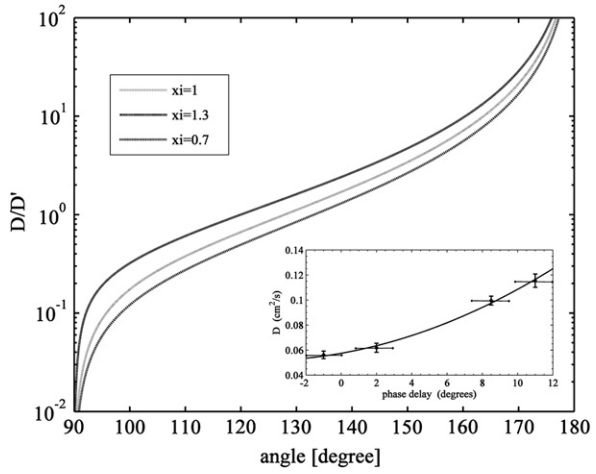

Fig. 4. Dependence of the normalized thermal diffusivity with the phase delay evaluated for three pump and probe normalized separations xi. The inset shows the experimental correlation between the thermal diffusivity and the phase delay at fixed frequency and beam displacement xi. The fit to the data is then used for calibration.

3. Results and discussion:

In order to show how two-dimensional scans can be correlated to hardness, in the first place we will plot in a different manner other author's prior work, so that the correlation becomes evident at a submilimeter scale (Section 3.1). Following this scheme we will show that the correlation is maintained also at a micrometer scale comparing a line scan of the inverse of the diffusivity with the hardness measured with a nano-indenter. Moreover, it will be shown that plotting the data as increments with respect to values of the base material, a single unique linear correlation is obtained despite the two orders of magnitude difference in spatial scale used here and in previous works. Finally using these results for calibration the two-dimensional map of hardness is retrieved and discussed.

3.1. Correlation between hardness and diffusivity

3.1.1. Prior work

As mentioned in the Introduction, in the past decade several groups have reported the correlation between thermal transport and hardness in the millimeter range in surface treated steel samples [3–12]. In all cases a monotonous decrease in thermal diffusivity or conductivity was found as hardness increases. The technique relies in the measurement of the surface temperature frequency dependence when the sample is heated by a modulated beam. The modulated beam impinges the surface and heat diffuses towards the substrate. The penetration in one modulation period depends on thermal diffusivity; lower frequencies explore deeper layers. An inversion algorithm recovers the diffusivity profile from the frequency dependence of the surface temperature rise.

We have converted the reported results and plotted the inverse of the thermal diffusivity as a function of the measured hardness using data from eight different works (Fig. 5). The data correspond to different treatment methods, different base alloys and range from pearlitic or ferritic structures at the lower side of the hardness axis to samples with high martensite content at the other side of the plot. A quite linear increase is detected in all cases with very similar slopes but with curves displaced vertically depending on the departing structure. As in all cases a surface treatment was performed, the low end of each curve corresponds to the data deeper in the sample where the material was not hardened, i.e. the departing material (base material). Some samples were hardened by laser quenching, others by carburizing or even a combination of both. It is an expected result to find that an increase in defects introduced by carburizing increases hardness and simultaneously hinders heat transport, increasing the

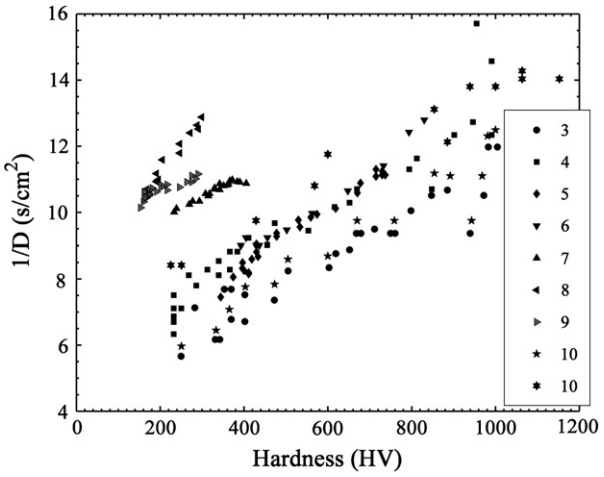

Fig. 5. Plot of 1/D vs. hardness with the data taken from prior works. The numbers for each data set indicate the reference from which the data were obtained [3–10].

inverse of diffusivity. On the other hand, as martensite has a larger hardness and a lower thermal diffusivity than ferrite, it is also expected to find that a larger martensite fraction increases hardness and reduces thermal diffusivity. What is somewhat surprising is that both mechanisms combined yield an almost linear dependence of the inverse of diffusivity with hardness.

3.1.2. Line scan: calibration

The cross section of the treated region was scanned along a line both for hardness and thermal diffusivity. The results are shown in Fig. 6. Indentations for hardness measurement can be visualized in the photograph (Fig. 6a). They were performed following a rectangular grid with 5 μm by 10 μm spacing. This distance is necessary because each test induces deformations in the surroundings that impede dense packing determinations. The results shown in the plot of Fig. 6b are dense thanks to the small tilt between the grid and the sample surface, allowing a small change in the sampled depth for each line. Optical measurement does not need the use of such tricks, as the determination does not affect the sample and dense scans can be performed along a line, with a 1 μm step in this case. The inverse of thermal diffusivity is plotted in Fig. 6c. It can be observed that the change of 1/D from the nickel layer to the hard treated steel layer, that should be sharp, has a trend with a spatial variation in a range of the order of the 3.6 μm pump beam spot size (circle in the figure) indicating the spatial resolution of the setup and the objective used (10× Mitutoyo long working distance objective). The probe beam was focused to a smaller size (2.8 μm). The slow decrease from the hard layer towards the base material does correspond to a real feature, indicating a transient region that could not be resolved with the nanoindenter.

A correlation is observed between hardness and thermal diffusivity (Fig. 6d) similar to that of prior works shown in Fig. 5 at millimeter scale. The correlation between the inverse of thermal diffusivity and hardness does not hold for the nickel layer and has only been found for different steel phases and thermally treated structures.

To show the strong correlations at a micrometer scale we will define the incremental magnitudes as:

$$\Delta H = H - H_{\text{base}} \tag{5}$$

$$\Delta\left(\frac{1}{D}\right) = \frac{1}{D} - \frac{1}{D_{\text{base}}} \tag{6}$$

which correspond to the increase in the magnitude respect to the base material (H_{base} and D_{base}). Our data from Fig. 6d are converted from GPa to HV (1 GPa = 0.009807HV [1,23]) for comparison with prior works, and plotted in Fig. 7 together with the data from Fig. 5 recalculated according to Eqs. (5) and (6). A least square fit was performed for prior works data and is shown in the figure together with the Fig. 6d data, showing a unique linear correlation. From this correlation the hardness increase due to the treatment can be retrieved from the measurement of the increase in the inverse of the diffusivity, and the hardness can be reconstructed from a single measurement of the hardness of the base material before surface treatment. As mentioned before this correlation is quite surprising although some physical insight can be given. The increase in hardness is obtained by introducing defects and imperfections in the lattice by means of precipitates, grain boundaries, etc. It is also obtained by increasing the martensite content. The increase in boundaries and defects hinders the transport of phonons and electrons, and hence increases the resistivity (as inverse of the conductivity). This is the relation between hardness increase and inverse of thermal diffusivity. The martensite phase also has a lower conductivity, and hence has a similar effect in the correlation between hardness increase and diffusivity: more martensite means more resistivity and more hardness. Surprisingly the two mechanisms yield similar quantitative results and hence the single measurement of the inverse of the thermal diffusivity change yields information on the hardness increase, irrespective to which is the hardening mechanism.

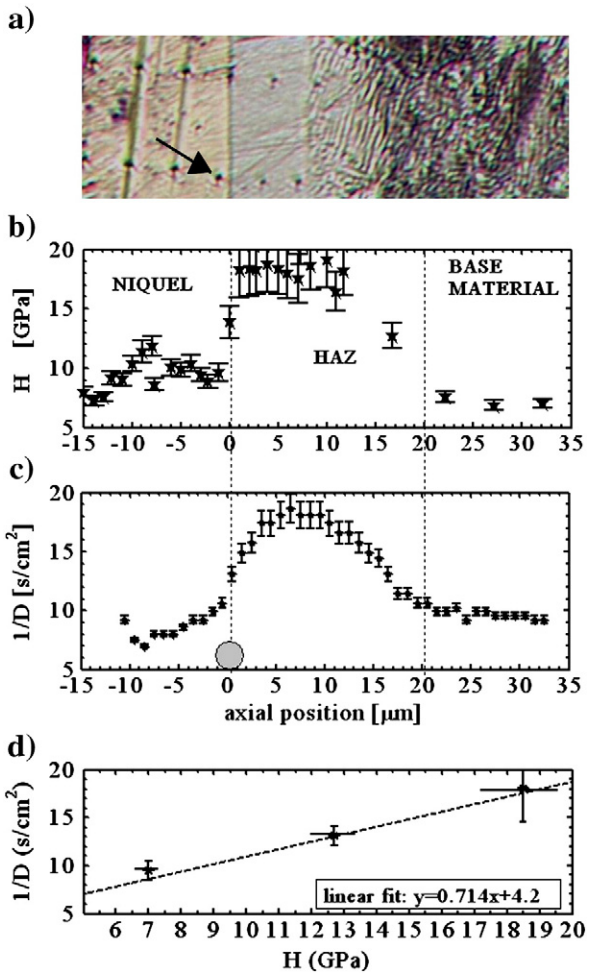

Fig. 6. a) Cross section of the sample tested with the nanoindenter following a tilted grid sequence. The arrow shows one of the indentations. b) Hardness obtained along the depth coordinate. c) Measured 1/*D* by the photodeflection method in the same region d) Measured correlation between the inverse of the diffusivity and hardness.

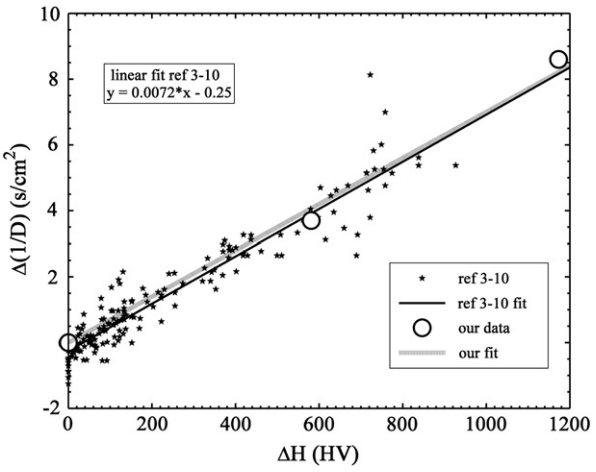

Fig. 7. Plot of Δ(1/*D*) (Eq. 6) vs. hardness increase (Eq. 5) Data taken from references 3–10 (*), linear fit (solid line), our data (O) and linear fit (–) from Fig. 6d. A strong linear correlation of all data is evident despite the difference in treatment method and spatial scale.

3.2. Two-dimensional scans

Following the procedure presented in [14] and described in Section 2.2 the diffusivity could be retrieved with a single measurement of the phase delay of the photothermal signal at a single frequency. In this manner a full two-dimensional scan was performed keeping constant beam sizes and separation. The measurements shown in Fig. 8 were obtained at a modulation frequency of 700 kHz. At this frequency a 2 ms integration time per point was used to retrieve the entire map with a one degree error in the phase delay. Ten times faster scan speeds are possible with an error around 2 to 3 degrees. Fig. 8a presents the phase delay map, converting the phase delay to diffusivity (Fig. 4) and using the data from Fig. 6d for calibration, the two-dimensional hardness map can be obtained and is presented in Fig. 8b.

A similar scan at an adjacent area is shown in Fig. 9. Here an anomalous region with a higher phase delay (higher diffusivity) appears in the rapidly quenched layer (see data around coordinates $x=25$ μm and $y=-23$ μm). The optical image (Fig. 10a) covering both regions corresponding to the maps presented in Figs. 8a and 9 and the scanning electron microscope (SEM) image of the same zone (Fig. 10b) did not show any particular feature in this region.

After locating the exact zone of the anomaly in the SEM image, two line scans of carbon content by energy dispersive spectroscopy (EDS) were performed (named AB and CD in Fig. 10b). When the line scan crossed the region of anomalous diffusivity a threefold increase in carbon concentration was detected (Fig. 11a and b).

It must be recalled that this sample was not carburized for hardness increase but instead was rapidly quenched from the melt. The carbon content did not correlate to an increase in hardness, but instead to a decrease, probably because the increase in the carbon content was already present in the melt and hindered the formation of the martensite in this region. This anomaly cannot be rapidly detected by any other method as it would have required an element by element detailed map by EDS. The warning given by the photothermal technique allowed the detailed EDS scan at the proper site without needing a two-dimensional element map in the entire sample. Notice that a smaller anomaly also appears in Fig. 8a at coordinates $x=35$ μm and $y=-25$ μm, and EDS carbon scan line reaches that region also

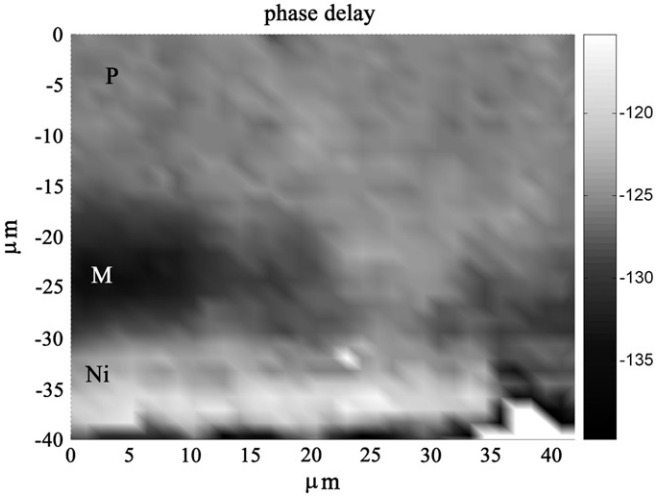

Fig. 9. A scan at an adjacent area of Fig. 8a. Note an anomaly at approximately $x=25$ μm and $y=-23$ μm in the rapidly quenched layer. This anomalous behavior was not detected by the other techniques employed.

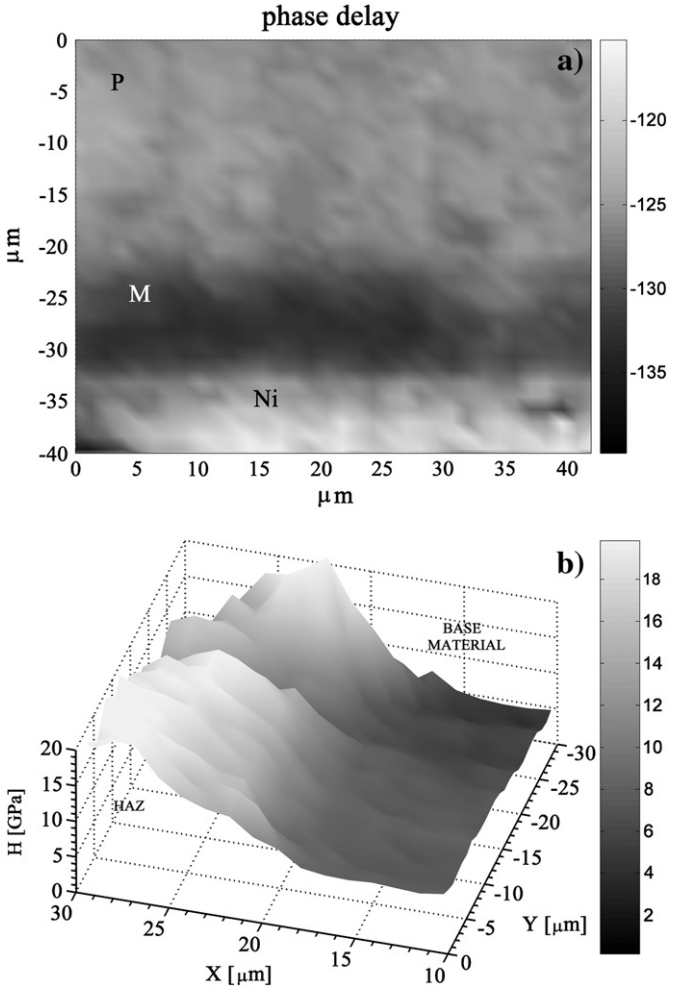

Fig. 8. a) Two-dimensional scan of phase delay for a cross section of the treated material. Note that distinct phases are revealed: the Ni layer added for flatness after polishing, a hardened martensite layer (M) and the pearlite structure (P) from the base material. b) Two-dimensional hardness map obtained from the calibration provided by data shown in Figs. 4 inset and 6d.

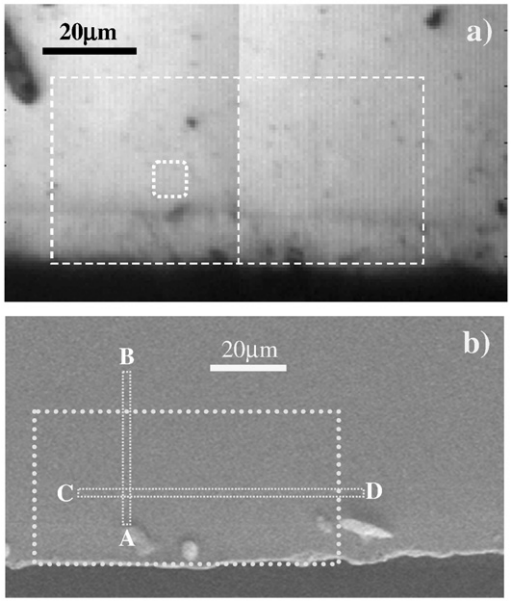

Fig. 10. The two regions explored in Figs. 8a and 9 observed with other techniques (rectangles in figures). No particular feature was observed in the region identified as abnormal by the photothermal technique (dotted square in a). a) Optical image (composed micrograph). b) Scanning electron microscope image. AB and CD indicate the lines scanned by EDS and shown in Fig. 11.

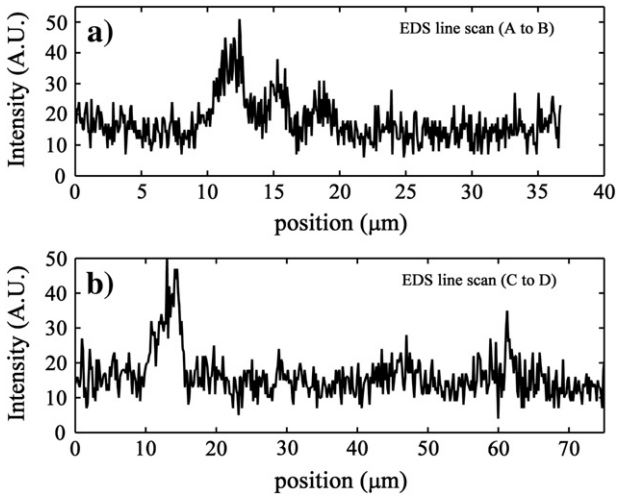

Fig. 11. A line scan of Carbon content by energy dispersive spectroscopy (X ray fluorescence) across the region depicted in Fig. 10b. a) Line AB b) line CD. A threefold increase in carbon concentration was found in the anomalous region.

showing an increase in carbon content, but barely above the noise (coordinate 60 μm in CD line in Fig. 11b).

4. Conclusions

An optical noncontact technique was presented that provides a two-dimensional map of hardness increase of treated steel at the micrometer level. This is possible due to the linear correlation for this type of material between the inverse of the diffusivity and the hardness. By plotting the inverse of the thermal diffusivity vs. the hardness from results extracted from prior works it was shown that this correlation appears in different steels hardened with different techniques at the sub-millimeter scale and that the linear relation between the inverse of the diffusivity and hardness persists even when different crystallographic phases are present. There is no substantial change in the slope with the change in the base material, and a shift in the ordinate at the origin is detected from one particular departing alloy to another. This same linear relationship was shown to persist at the micrometer level. When plotting the change in the inverse of the thermal diffusivity as a function of the change in the hardness (referred to the untreated material) a universal straight line was found irrespective of the particular steel and hardening treatment used. The same curve fits prior data at the millimeter range and our new results at the micrometer range. With a single measurement of the hardness of the departing material the hardness map can be retrieved optically without the need of further calibration. Although the correlation has only been proved for hardened steels, it might be expected to appear in other metals if hardened by introducing precipitates or other lattice defects.

The photodeflection technique for determining thermal diffusivity was in this manner shown to be a useful and rapid way to determine the hardness profile in two dimensions with only minor preparation of the sample (flat polish). The diffusivity retrieval presented in a recent work [14] was used in this case for a rapid scanning of the surface without the need for a frequency scan at each point in order to recover the thermal diffusivity. The phase delay between the modulation and the measured signal provides all the required information after performing a calibration for the particular frequency, beam sizes and separations.

The hardness surface scans showed that anomalous regions can be identified that direct optical or SEM observation do not reveal. After locating the anomalous regions, detailed spectroscopic studies focused to that area, allowed the recognition of the origin of the anomaly. The EDS scan speed was 1000 times slower (2 s/point) than that the photothermal method (2 ms/point). Direct mapping of all elements with EDS with the required resolution and sensitivity is otherwise prohibiting as an inspection tool.

References

[1] W.C. Oliver, G.M. Pharr, J. Mater. Res. 7 (1992) 1564.
[2] D. Brandon, W.D. Kaplan, Microstructural characterization of materials, Second edition. J.Wiley & Son Ltd., Chichister, England, 2008.
[3] T.T.N. Lan, U. Seidel, H.G. Walther, G. Goch, B. Schmitz, J. Appl. Phys. 78 (1995) 4108.
[4] A. Mandelis, M. Munidasa, L. Nicolaides, NDT and E Int. 32 (1999) 437.
[5] J.C. Krapez, J. Appl. Phys. 87 (2000) 4514.
[6] J.C. Krapez, R. Li Voti, Anal. Sci. 17 (Special Issue) (2001) s417.
[7] L. Nicolaides, A. Mandelis, C.J. Beingessner, J. Appl. Phys. 89 (2001) 7879.
[8] K.M. Boubaker, M. Bouhafs, N. Yacoubi, NDT and E Int. 36 (2003) 547.
[9] Liu Yue, N. Baddour, A. Mandelis, C.J. Beingessner, J. Appl. Phys. 96 (2004) 1521.
[10] D. Kruse, H. Prekel, G. Goch, H.G. Walther, Proc. Est. Acad. Sci. Eng. 13 (2007) 423.
[11] L. Nicolaides, A. Mandelis, J. Appl. Phys. 90 (2001) 1255.
[12] Qu. Hong, Wang Chinhua, Guo XinXin, A. Mandelis, J. Appl. Phys. 104 (2008) 113518.
[13] O.E. Martínez, F. Balzarotti, N. Mingolo, Appl. Phys. B 90 (2008) 69.
[14] U. Crossa Archiopoli, N. Mingolo, O.E. Martínez, J. Appl. Phys. (2010) 023520.
[15] Y. Cesa, N. Mingolo, O.E. Martínez, IEEE Trans. Plasma Sci. 28 (2000) 1035.
[16] N. Mingolo, Y. Cesa, O.E. Martínez, J.I. Etcheverry, J.J. Rocca, IEEE Trans. Plasma Sci. 28 (2000) 386.
[17] N. Mingolo, C.R. González, O.E. Martínez, J.J. Rocca, J. Appl. Phys. 82 (1997) 4118.
[18] P. Marino Belçaguy, N. Mingolo, O.E. Martínez, IEEE Trans. Plasma Sci. 31 (2003) 788.
[19] U. Crossa Archiopoli, N. Mingolo, O.E. Martínez, Metall. Mater. Trans. A 36 (2005) 999.
[20] N. Mingolo, A.N. Roviglione, O.E. Martínez, J. Mater. Res. 16 (2001) 2343.
[21] M. Bauccio (Ed.), ASM Metals Reference Handbook, 3rd, ASM International, Materials Park, OH, 1993, p. 318.
[22] U. Crossa Archiopoli, N. Mingolo, N. Mingolo, Surf. Coat. Technol. 202 (2008) 5982.
[23] ASTM E 384-99, Standard Test Method for Microhardness of Materials, ASTM Annual Book of Standards, 3.01, 2000.